Available online at www.sciencedirect.com

jmr&t Journal of Materials Research and Technology

journal homepage: www.elsevier.com/locate/jmrt

Original Article

Synergetic grain refinement and ZrB_2 hardening in in-situ ZrB_2/AA4032-type composites by ultrasonic assisted melt treatment

S. Chankitmunkong [a], D.G. Eskin [b,c], C. Limmaneevichitr [d], P. Pandee [d,e,*]

[a] Department of Industrial Engineering, School of Engineering, King Mongkut's Institute of Technology Ladkrabang, Chalongkrung Road, Ladkrabang, Bangkok 10520, Thailand
[b] Brunel University London, BCAST, Uxbridge, Middlesex UB8 3PH, United Kingdom
[c] Tomsk State University, Tomsk 634050, Russian Federation
[d] Department of Production Engineering, Faculty of Engineering, King Mongkut's University of Technology Thonburi, 126 Pracha-Utid Rd., Bangmod, Tungkhru, Bangkok 10140, Thailand
[e] Center for Lightweight Materials, Design and Manufacturing, King Mongkut's University of Technology Thonburi, 126 Pracha-Utid Rd., Bangmod, Tungkhru, Bangkok 10140, Thailand

ARTICLE INFO

Article history:
Received 14 February 2023
Accepted 24 March 2023
Available online 29 March 2023

Keywords:
Al–Si alloy
Aluminum matrix composites
Nanoparticle-reinforcement
Grain refinement
In-situ particles

ABSTRACT

In this work, the effects of ultrasonic treatment on in-situ ZrB_2 particle-reinforced AA4032-based composites were studied. The composites were synthesized from Al–K_2ZrF_6–KBF_4 system via an in-situ melt reaction. The phase composition, macrostructure characteristics, hardness and tensile properties of the composites were investigated. The results showed that the addition of in-situ submicron ZrB_2 particles into the composites resulted in grain refinement, and the increased hardness and tensile properties. The ultrasonic treatment effectively enhanced the uniformity of in-situ ZrB_2 distribution, which further enhanced the structure and mechanical properties of the composites. The mechanisms of the ultrasonic treatment in the improvement of in-situ particle distribution and mechanical properties of the composites were discussed.

1. Introduction

AA4032 is a near-eutectic Al–Si based alloy that is widely used for automotive applications such as pistons and scroll compressors due to its good mechanical properties at high temperatures. Previous studies reported that an addition of 3.5 wt % Cu to an AA4032 alloy improved the hardness and tensile strength [1]. The higher Cu content led to the formation of thermally stable Cu-rich phases, i.e., γ-Al_7Cu_4Ni, δ-Al_3CuNi and Q-$Al_5Cu_2Mg_8Si_6$, which increased the high-temperature properties for engine application [2–4]. Nowadays, in-situ aluminum matrix composites (AMCs) have attracted great interest, having the advantages of finer reinforcement, good thermodynamic stability and strong interfacial bonding

* Corresponding author.
E-mail address: phromphong.pan@kmutt.ac.th (P. Pandee).
https://doi.org/10.1016/j.jmrt.2023.03.182

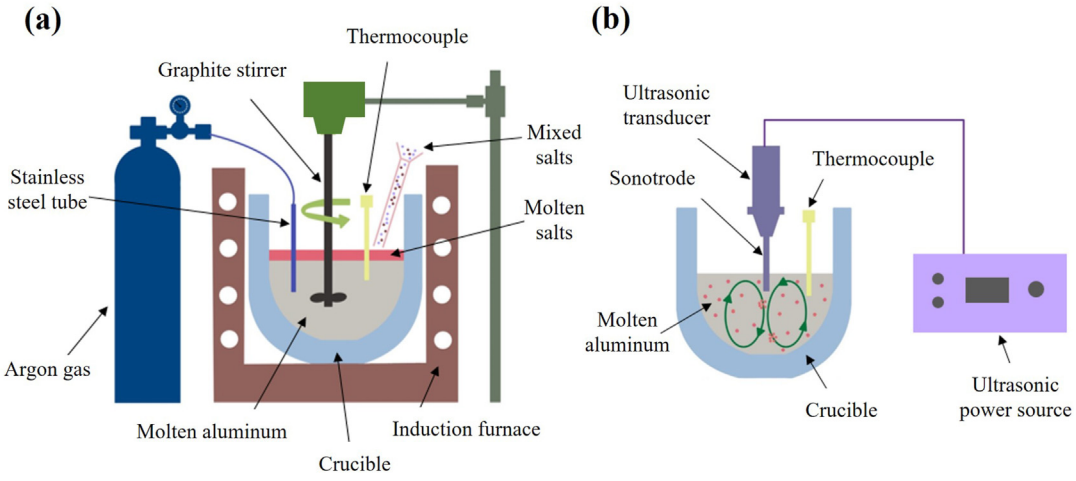

Fig. 1 – Schematic diagrams of the synthesis of AA4032-3.5Cu–ZrB_2 composites by (a) mechanical stirring and (b) additional ultrasonic treatment.

between the particle and the matrix as compared with the ex-situ ones [5]. Different particles, such as titanium diboride (TiB_2), zirconium diboride (ZrB_2), titanium carbide (TiC), and alumina (Al_2O_3) were suggested as potential in-situ particles for producing aluminum matrix composites. Among the particles, ZrB_2 is a promising candidate due to its excellent properties, i.e., high melting temperature, high hardness, good corrosion resistance and high wear resistance [6,7]. ZrB_2 particles have also a positive effect on dimensional stability, which is critical for engine applications [8]. Recently, a number of aluminum alloys based composites reinforced with in-situ ZrB_2 particles have been developed, i.e., AA2024 [9], AA5052 [10], AA6061 [11], AA6111 [12,13], AA7075 [14], ADC12 [15] and A356 [16]. The addition of in-situ ZrB_2 reinforcement was shown to improve not only the tensile strength of aluminum alloy but also other properties, i.e., creep resistance [17], wear resistance [15,18], and fatigue performance [12]. However, there is lack of research in the in-situ ZrB_2 composites with high-Si alloys as a matrix, which can be attractive for engine applications.

Clustering of in-situ particles inside the metal matrix is a typical issue encountered during the manufacture of composites using stir casting processes. To disperse the clusters, some external force must be applied. Ultrasonic treatment (UST) is considered as an effective technology for degassing molten metals and refining the microstructure [19]. Moreover, it was reported that the UST can effectively disperse particles due to acoustic cavitation and streaming [20]. It was also reported that the UST can improve the uniformity of distribution of in-situ particles, i.e., Al_3Ti [21], Al_3Zr [22], TiB_2 [23,24], Al_2O_3 [25], ZrB_2 [26] and $MgAl_2O_4$ [27] in aluminum matrix composites. UST was demonstrated to enhance both particle

Table 1 – The chemical compositions of the experimental alloy and composites (wt%).

Alloys	Si	Mg	Cu	Ni	Fe	Zr	B	Al
AA4032-3.5Cu	12.15	0.83	3.57	0.55	0.40	–	–	Bal.
AA4032-3.5Cu–ZrB_2	12.24	0.87	3.52	0.58	0.47	2.68	0.57	Bal.
AA4032-3.5Cu–ZrB_2+UST	12.23	0.85	3.55	0.57	0.49	2.61	0.57	Bal.

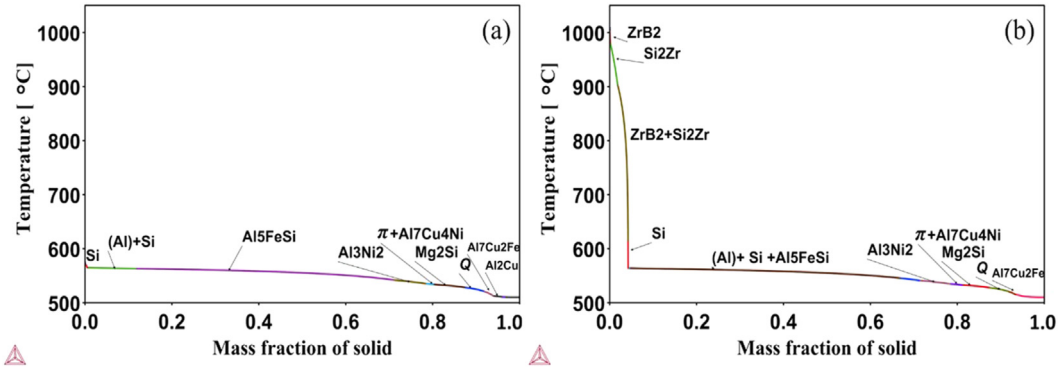

Fig. 2 – Scheil simulation of phase formation in (a) the base alloy and (b) the composite; only the phases that are formed in the solidification ranges are shown.

dispersion and in-situ particle formation, ultimately increasing the particle count in the matrix [26,28]. Previous works have studied the in-situ formation of ZrB_2 by salts synthesis [17], and the effect of UST on nanoparticle dispersion and grain refinement [29]. However, due to the complex chemical composition and phase formation in an AA4032-type alloy, the in-situ ZrB_2/AA4032 composite synthesized through a combination of stir process and UST deserves to be studied in detail.

Thus, to gain insight into the mechanism of phase formation by the combined effect of salt synthesis with stir process and UST, and the corresponding effects on the structure and mechanical properties, in this study an AA4032 alloy with high Cu content (3.5 wt%) reinforced with ZrB_2 particulates was prepared by the in-situ reaction of K_2ZrF_6 and KBF_4 salts with the melt assisted with mechanical stirring. The composites then were processed with UST before casting. The macrostructure, microstructure and mechanical properties of the composites were investigated, and the effects of UST were discussed.

2. Experimental procedure

An AA4032-type alloy used in this study was prepared from 99.7 wt% pure Al, 99.9 wt% pure Si, 99.5 wt% pure Mg, 99.9 wt% pure Cu, and Al-20 wt% Ni and Al-10 wt% Fe master alloys. The AA4032-type alloy contained 3.5 wt% Cu, as shown in our previous research, improves mechanical properties at room and elevated temperature [1]. AA4032-type ingots were produced in an induction furnace at a temperature of 700 °C. Then, AA4032-type ingots were remelted to mix with salt flux for the in-situ synthesis reaction to make composites. The in-situ ZrB_2 reinforced particles were synthesized through the chemical reaction of K_2ZrF_6 and KBF_4 salts with the aluminum melt [10,14]:

$$3K_2ZrF_6 + 13Al \rightarrow 3Al_3Zr + 4AlF_3 + 6KF \quad (1)$$

$$2KBF_4 + 3Al \rightarrow AlB_2 + 2AlF_3 + 2KF \quad (2)$$

$$Al_3Zr + AlB_2 \rightarrow ZrB_2 + 4Al \quad (3)$$

The two salts were preheated at 300 °C for 3 h in an electric oven to remove the bonded water contained therein, and then were mixed together mechanically. An AA4032-3.5 Cu ingot with a weight of about 1800 g was melted in a silicon carbide crucible and maintained at 850 °C by using an induction furnace with a heating and cooling controller. The mixed salts were added manually to the molten alloy with the amount reflecting 5 wt% ZrB_2 to be produced with the ratio of K_2ZrF_6 235 g and KBF_4 205 g in the molten aluminum of 1800 g. The melt was stirred for 30 min by a high-purity graphite impeller stirrer, maintaining the liquid temperature at 850 °C. The experimental system is shown in Fig. 1a. After the salt synthesis reaction was completed, the liquid by-products in the top layer of the melt were collected. After removing the by-products, the composite melt was degassed by purging pure argon gas. To study the effect of UST, after the salt reaction was completed for 30 min and the molten metal cleaned, the ultrasonic vibration with a power of 1.5 kW (an air-cooled piezoelectric transducer) and a frequency of 20 kHz was introduced for 3 min to the composite melt through a preheated Nb sonotrode with a diameter of 20 mm, as illustrated in Fig. 1b. The liquid metal temperature was maintained during the UST at 720-680 °C. The same procedure was repeated for composites without UST. Then the composite melt was poured into a steel mold (150 mm × 170 mm × 15 mm) at 680 °C. The chemical compositions of the studied alloys were analyzed after melt in-situ synthesis reaction using optical emission spectrometry and are given in Table 1. Thermo-Calc software (version 2023a) with the TCAL8 database was utilized to define the sequence of phase formation in the composite, which contains 2.68 wt% Zr and 0.57 wt% B after the in-situ ZrB_2 reaction.

Specimens were machined from the castings for structure and mechanical characterization. The specimens were polished following standard metallographic procedures and etched with Keller's reagent (5 ml HNO_3, 3 ml HCl and 2 ml HF in 190 ml distilled water), and then examined by optical microscopy (Olympus DSX1000). To reveal their grain structures, specimens were anodized in Barker's agent (5% HBF_4 water solution) for about 2 min at 20 V and were then examined by the Olympus microscope with polarized light. The grain size was measured by the linear intercept method (ASTM E112-10). Moreover, the specimens were examined using a field emission scanning electron microscope (FE-SEM, Thermo Scientific

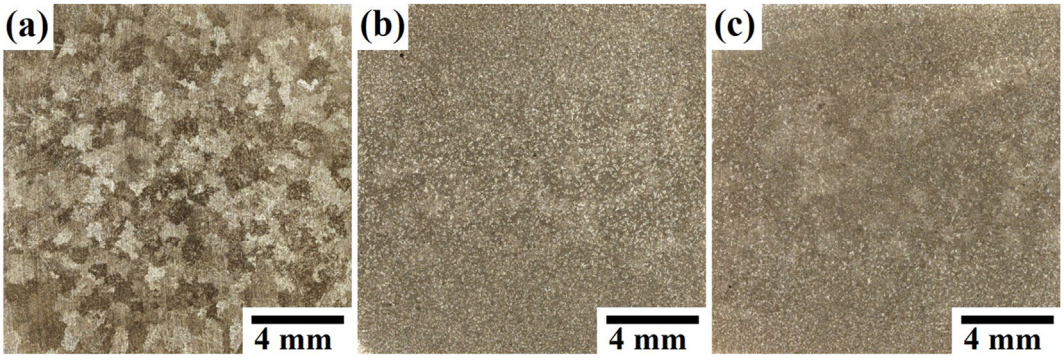

Fig. 3 – Optical macrographs of the alloy and composites: (a) AA4032-3.5Cu, (b) AA4032-3.5Cu–ZrB_2, and (c) AA4032-3.5Cu–ZrB_2 with UST.

Apreo S) equipped with an energy-dispersive spectroscopy (EDS) detector. In addition, X-ray diffractometer (XRD, Bruker D8 advance) using Cu Kα radiation source was used to determine the phase composition of the specimens. The hardness of each specimen was measured using a Brinell hardness tester with a 2.5 mm ball indenter and 625 N load applied for 15 s. Each reported hardness value was the average of at least five indentations. Tensile specimens were prepared as per ASTM E8 standard having a gauge length of 40 mm, a gauge width of 7 mm and a thickness of 6 mm. The ultimate tensile strength (UTS), yield strength (YS) and percentage elongation (%El) were measured using a computerized universal testing machine at a cross head speed of 1 mm/s at 25 °C. Three samples for each group were tested to ensure the reliability of the results and the average values of YS, UTS and %El were calculated. The fracture surfaces of the tensile specimens were observed by FE-SEM to evaluate the fracture mechanisms of the composites.

3. Results

3.1. *Solidification sequence in an AA4032-3.5Cu composite containing ZrB_2*

Thermo-Calc software was utilized to define the solidification sequence of phase formation in the base AA4032-type alloy and the composite after the in-situ ZrB_2 reaction, as demonstrated in Fig. 2. The result showed that the ZrB_2 phase was formed in the composites from 1008 °C, followed by the formation of Si_2Zr phase at 980 °C, while the UST was performed between 720 °C and 680 °C, which is above the formation of primary Si at 613 °C. Therefore, the UST was performed in the range of Zr-phases formation and above the formation temperature of other phases.

3.2. *Microstructural characterization*

Optical macrographs showing the grain structure of the base alloy and the AA4032-3.5Cu–ZrB_2 composites are presented in Fig. 3. For a clearer presentation, optical micrographs using polarized light were produced, as displayed in Fig. 4. It is obvious in Figs. 3a and 4a that most grains in the base AA4032-type alloy have a dendritic shape with a rather large size (480 ± 4.2 μm). The grain structure of the AA4032-3.5Cu–ZrB_2 composite prepared with mechanical stirring without UST are presented in Figs. 3b and 4b. After the in-situ reaction of the generating ZrB_2 reinforcing particles, the grain size was significantly reduced. After applying UST, the grain size was further reduced, as shown in Figs. 3c and 4c, i.e., from 221 ± 2.0 μm to 138 ± 0.8 μm.

Optical micrographs at low and high magnifications of the matrix alloy and AA4032-3.5Cu–ZrB_2 composite are shown in Fig. 5. The addition of in-situ ZrB_2 into the AA4032-3.5Cu alloy refined and decreased the amount of primary Si particles, as well as refined the overall microstructure, as shown in Fig. 5a–e. Optical micrographs showing the eutectic Si morphologies in the matrix alloy and AA4032-3.5Cu–ZrB_2 composites are presented in Fig. 5d–f. The addition of in-situ ZrB_2 into the AA4032-3.5Cu alloy and the corresponding general refinement of the microstructure refined the eutectic Si from coarse plate-like (Fig. 5d) to lamellar morphologies (Fig. 5e) with its length decreasing from 4.8 ± 0.5 μm to 1.8 ± 0.5 μm. Moreover, UST further refined all microstructural features (Fig. 5c and f) and the length of eutectic Si decreased further with an average length of 0.6 ± 0.2 μm and more

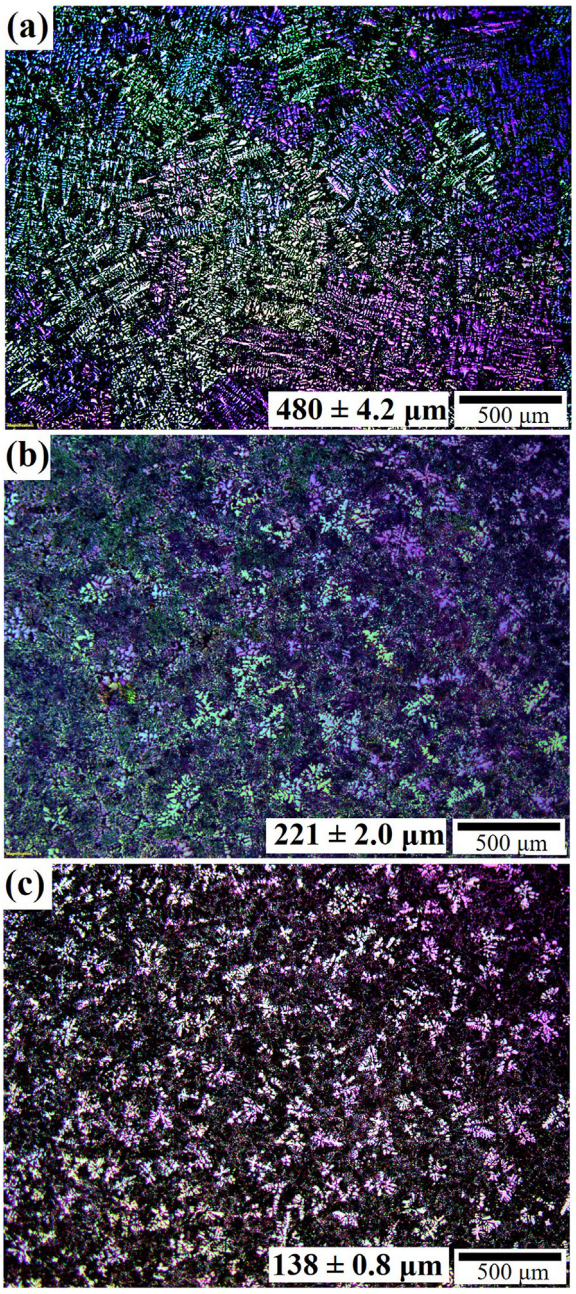

Fig. 4 – Polarized images showing the grain structure of the alloy and composites: (a) AA4032-3.5Cu, (b) AA4032-3.5Cu–ZrB_2, and (c) AA4032-3.5Cu–ZrB_2 with UST.

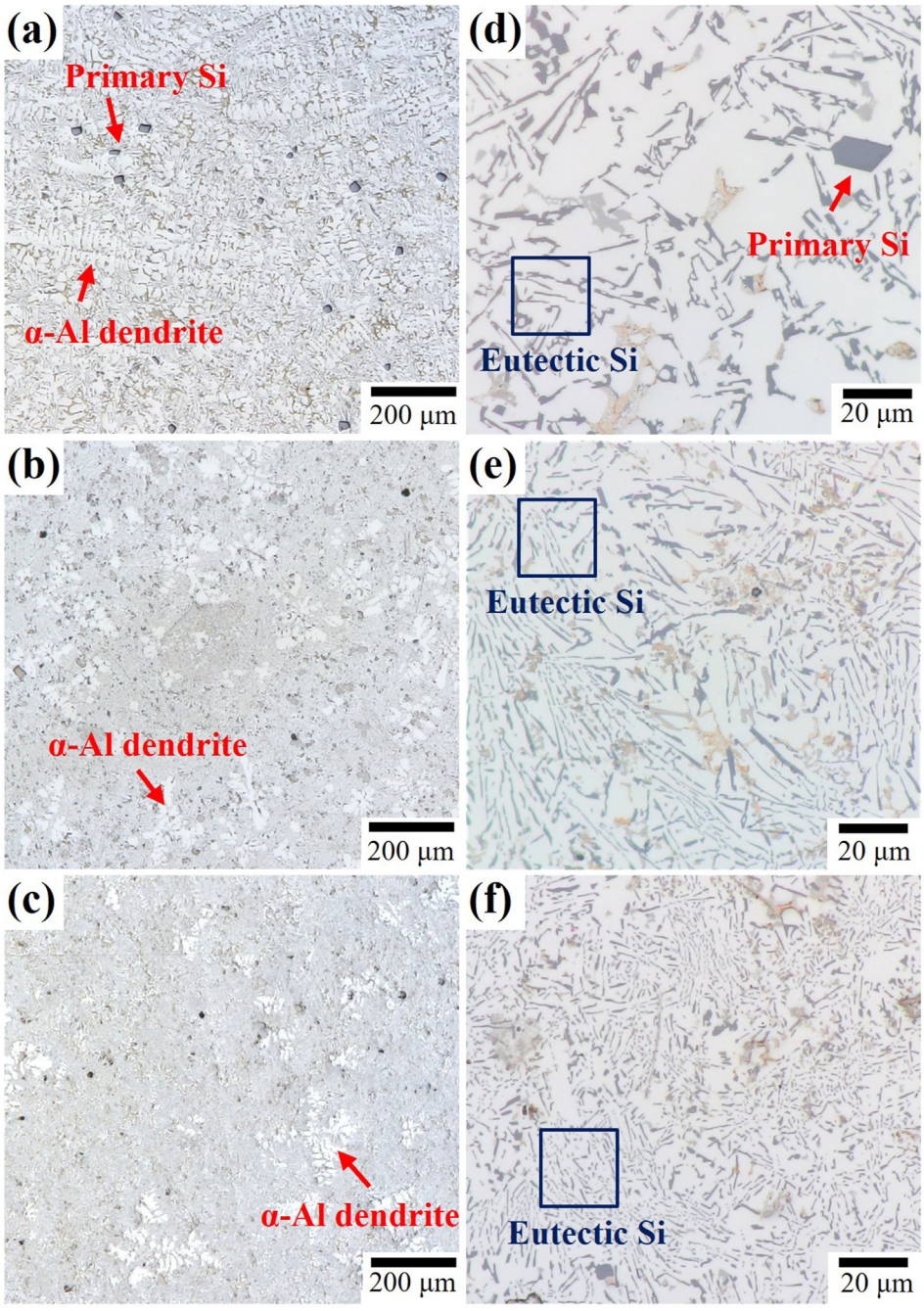

Fig. 5 – Optical micrographs of alloy and composites; at lower magnification: (a) AA4032-3.5Cu, (b) AA4032-3.5Cu–ZrB_2, (c) AA4032-3.5Cu–ZrB_2 with UST; and at higher magnification: (d) AA4032-3.5Cu, (e) AA4032-3.5Cu–ZrB_2, and (f) AA4032-3.5Cu–ZrB_2 with UST.

rounded morphology (Fig. 5f). The average size and area fraction of eutectic Si are shown in Fig. 6.

Fig. 7 shows SEM micrographs of the base alloy and AA4032-3.5Cu–ZrB_2 composites. In-situ addition of Zr and B resulted in the increased heterogeneity of the structure with possible suppression or significant refinement of primary Si. The microstructure of composites (Fig. 7b and c) contained ZrB_2 and Si_2Zr phases. It is also found that Si_2Zr was finer after UST, as shown in Fig. 7d and e. The element mapping in Fig. 8 confirmed the presence of Zr and Si elements, which were expected to be Si_2Zr phase, and the composition of the ZrB_2 particles was confirmed by the semi-qualitative EDS analysis

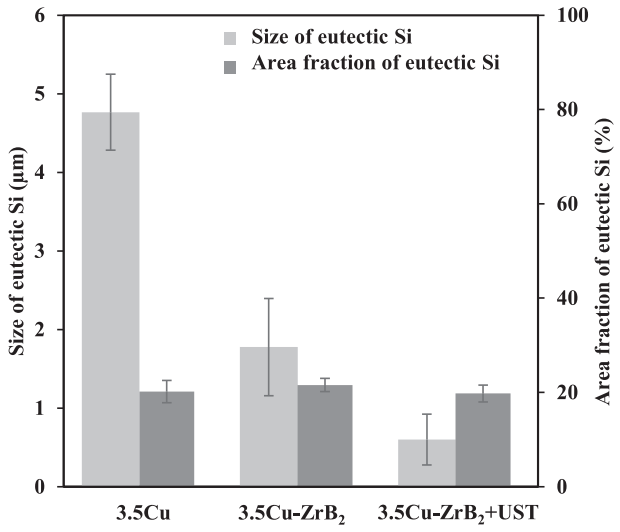

Fig. 6 – Size and area fraction of eutectic Si in the tested alloy and composites.

as shown in Fig. 9. This result is consistent with the XRD results presented in Fig. 10. There are diffraction peaks of Al and Si, which are the main phases contained in the AA4032 base alloy. The XRD pattern also confirms the successful formation of the ZrB_2 phase in the composite through a direct in-situ melt reaction technique between the salts K_2ZrF_6 and KBF_4 in the molten AA4032. ZrB_2 particles clustered in the microstructure with agglomerate sizes of 10 ± 5 μm, while the small individual particles observed by SEM, were 200 ± 20 nm in size as shown in Fig. 9b. In general, the experimentally observed phase composition agreed well with the results of thermodynamic calculations in Fig. 2.

Fig. 11 shows the ZrB_2 particles distribution in AA4032-3.5Cu prepared without and with UST. These data further confirmed that UST increased the uniformity of distribution of ZrB_2 particles in the aluminum matrix with less agglomeration. This is quantified by the frequency distribution that shows more individual fine particles after UST (Fig. 11f).

3.3. *Mechanical properties*

The hardness of the base alloy and the AA4032-3.5Cu–ZrB_2 composites was determined using the Brinell method and the average hardness results are shown in Fig. 12. As expected the hardness increased with the in-situ ZrB_2 reinforcement. Ultrasonic treatment of the AA4032-3.5Cu–ZrB_2 composite further increased the hardness and decreased the scatter of the results (evidenced by a smaller standard deviation), indicating that the UST made the structure more homogenous.

The average yield strength (YS), ultimate tensile strength (UTS), and percentage elongation (%El) of the base alloy and AA4032-3.5Cu–ZrB_2 composites are given in Fig. 13. The tensile properties of the alloy increased with the addition of the in-situ ZrB_2 reinforcement. Interestingly, both strength and ductility showed the improvement, reaching YS of 151 MPa, UTS of 266 MPa, and El 1.9%.

The SEM fracture surfaces of the base alloy and AA4032-3.5Cu–ZrB_2 composites are shown in Fig. 14 There were numerous brittle planes and tearing edges in the fracture of the matrix alloy (Fig. 14a), which indicated that the main fracture mode of the AA4032-type alloy was cleavage. With the addition of ZrB_2 particles, the fracture surface exhibited more dimples and less tearing edges (Fig. 14b and c), which agreed with the better ductility.

The fracture surfaces of the AA4032-3.5Cu–ZrB_2 composites prepared without and with UST at a higher magnification are demonstrated in Fig. 15a and b, respectively. Large particle clusters of ZrB_2 can be seen in the AA4032-3.5Cu–ZrB_2 composite produced without UST, which will act as crack initiators, reducing the ductility as compared with the UST produced composite that has smaller and more evenly distributed agglomerates.

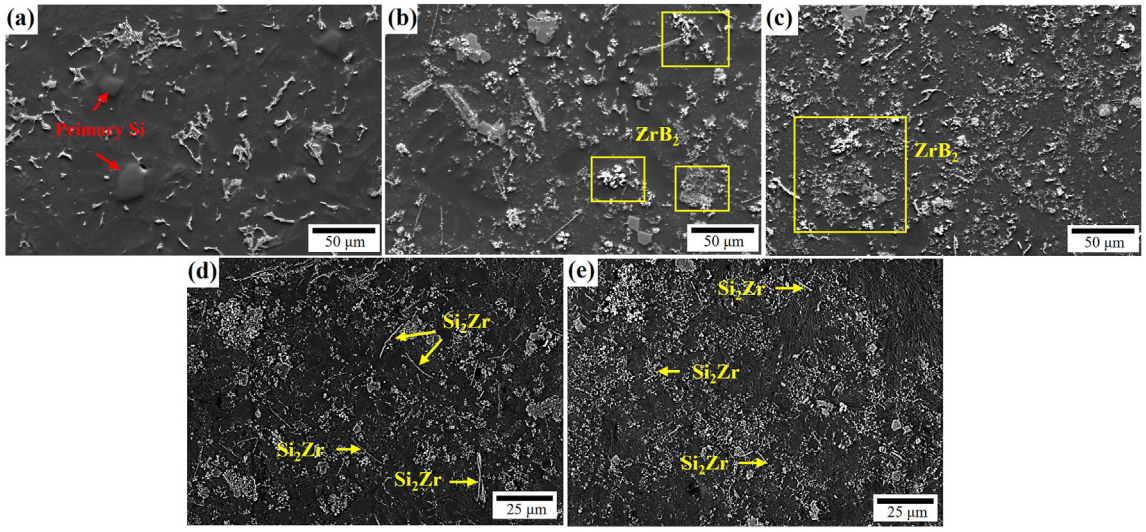

Fig. 7 – SEM micrographs of alloys and composites: (a) AA4032-3.5Cu, (b, d) AA4032-3.5Cu–ZrB_2, and (c, e) AA4032-3.5Cu–ZrB_2 with UST.

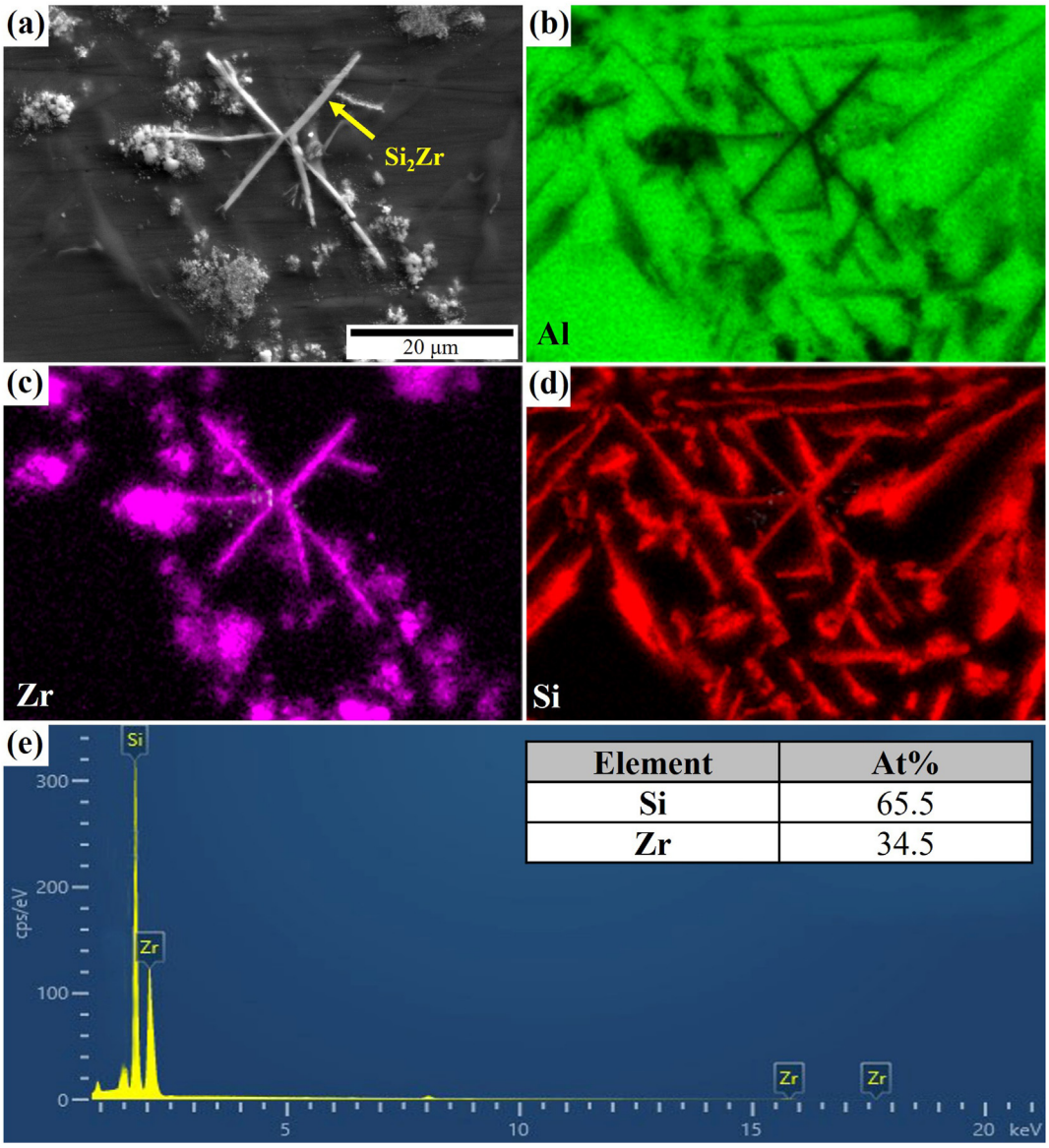

Fig. 8 – SEM image and EDS mapping analysis of Si_2Zr intermetallic in AA4032-3.5Cu–ZrB_2 composite prepared with UST.

4. Discussion

4.1. *Microstructure evolution in the composites after in-situ ZrB_2 synthesis*

We observed the decrease in the occurrence of primary Si after the in-situ formation of ZrB_2 phase. It was also observed that the Si_2Zr phase was formed with the Zr addition. EDS confirms that this phase contains Si and Zr elements, as showed in Fig. 8, which corresponding to thermodynamics of the ternary phase diagram in Ref. [30] as well as our thermodynamic calculations (Fig. 2). The formation of Si_2Zr phase may result in the decrease in the residual Si content in the melt and less Si available to form primary phase. Note that the base alloy is nearly eutectic, so the lack of available Si effectively shifts the alloy to hypoeutectic range. The observed grain refinement as a result of in-situ ZrB_2 formation (Figs. 3–5) agrees well with the previous work [9,10,14,31].

There are two mechanisms known to explain the grain refinement in metal matrix composites, i.e., the heterogeneous nucleation and the restricted grain growth. According to the heterogeneous nucleation mechanism, it is widely known that the lower the lattice mismatch of the solid/substrate, the greater the substrate particle nucleation potential. The crystal structure and lattice parameters of ZrB_2 are hexagonal close-packed a = 0.3172 nm, c = 0.3536 nm, and the lattice mismatch of ZrB_2 with Al (a = 0.4049 nm) is too large to

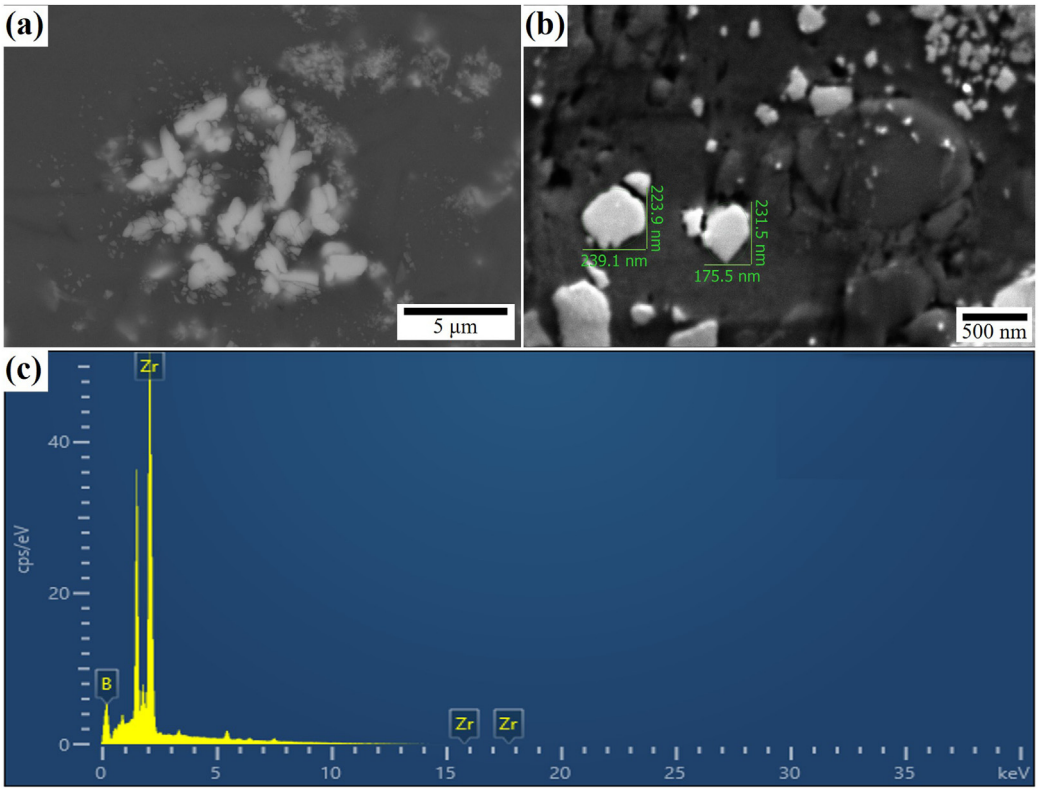

Fig. 9 – SEM images of AA4032-3.5Cu–ZrB_2 composite: (a) agglomerates, (b) nanoparticles of ZrB_2 and (c) EDS point analysis of ZrB_2 particles.

be a suitable nucleation site for Al matrix. ZrB_2 is known be an ineffective heterogeneous nucleating substrate for the Al matrix (hence Zr poisoning of TiB_2 grain refiners). Therefore, it can be suggested that the ZrB_2 particles pushed by the solid-liquid interface can limit the grain growth, resulting in the refining of grains and eutectic colonies during the solidification of ZrB_2/AA4032 composites [9,10,14,32].

The eutectic Si changed from a coarse plate-like to a lamellar morphology in the ZrB_2/AA4032 composite (Fig. 5), and the size significantly decreased (Fig. 6). The presence of in-situ ZrB_2 reinforced particles could hinder the growth of eutectic Si colonies as well, therefore the Si phase was refined [33,34]. In addition, residual potassium from the salt reaction can lead to partial modification of eutectic Si [35,36] as shown in Fig. 5.

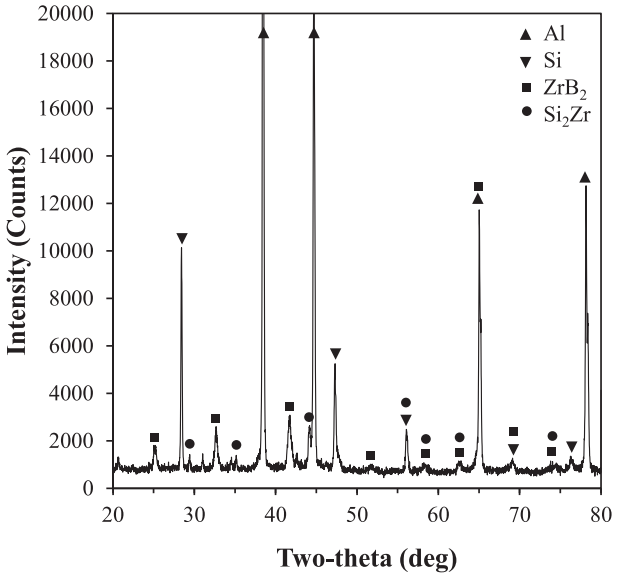

Fig. 10 – XRD patterns of AA4032-3.5Cu–ZrB_2 composites.

4.2. *The effect of UST on the evolution of microstructures*

As UST was performed in the range of ZrB_2 and Si_2Zr existence in the melt, these phases were directly affected by cavitation, which was evidenced by the deagglomeration of borides and refinement of silicides as shown in Figs. 7 and 11. The ZrB_2 particles tend to aggregate to form clusters as can be seen in Fig. 7b, leading to the nonhomogeneous distribution of particles (Fig. 11a–d). The mechanical stirring is unable to produce enough high shear force, which can break up these clusters completely, and the clustering of ZrB_2 particles unavoidably exists in aluminum matrix composites. A more uniform

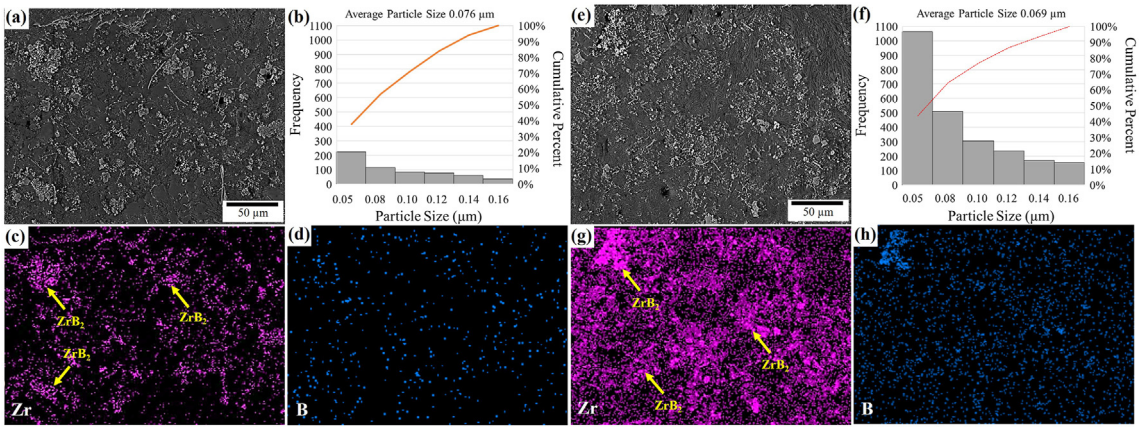

Fig. 11 – SEM images and EDS mapping analysis of the AA4032-3.5Cu–ZrB_2 composites prepared (a)–(d) without UST, and (e)–(h) with UST.

distribution of in-situ ZrB_2 reinforced particles can be observed in the SEM images of the composite with UST (Figs. 7c and 11e–f). The mechanisms involved in this phenomenon are well recognized as cavitation and acoustic streaming. The cavitation-induced deagglomeration and distribution of particles has been recently studied in detail [31]. The cavitation bubbles collapse in the liquid near the particle agglomerate and emit shockwaves that break up the agglomerates from the surface and from inside, while acoustic streaming disperses and distributes particles throughout the liquid metal. The further reduction in grain size may be attributed to the enhanced distribution of ZrB_2 particles that become more efficient in hindering the grain (eutectic colonies) growth. There is a possibility that UST also improves the nucleation potential of ZrB_2, though this needs to be studied additionally. The refinement of Si_2Zr particles upon UST is a result of fragmentation facilitated by the shock-wave emission upon cavitation as described in detail elsewhere [31].

4.3. *Strengthening mechanism*

The addition of ZrB_2 (and Si_2Zr) to the base alloy improved hardness, tensile strength and ductility, with UST giving some further improvement (Fig. 14). The increase of hardness was expected as both additional phases have high hardness, i.e. 14.5–25 GPa for ZrB_2 [37], and appr. 11 GPa for Si_2Zr [38]. The simultaneous increase in strength and ductility can be related to the soundness of the microstructure. The addition of hard particles to the already heterogeneous base alloy increased its

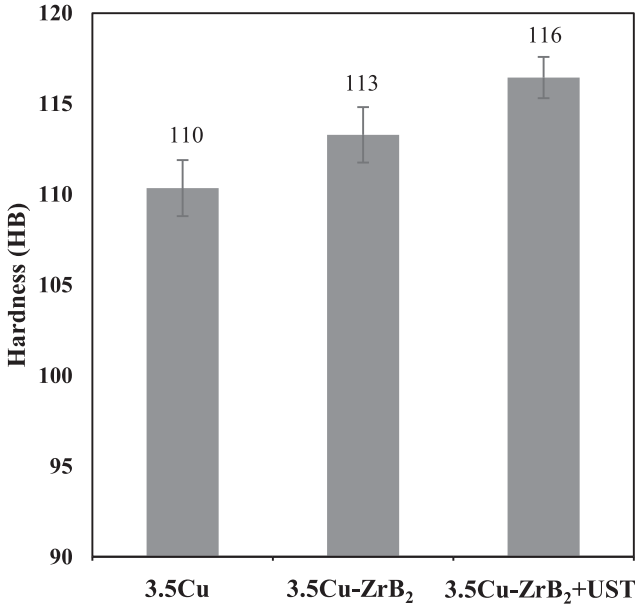

Fig. 12 – Brinell hardness of base alloy and AA4032-3.5Cu–ZrB_2 composites.

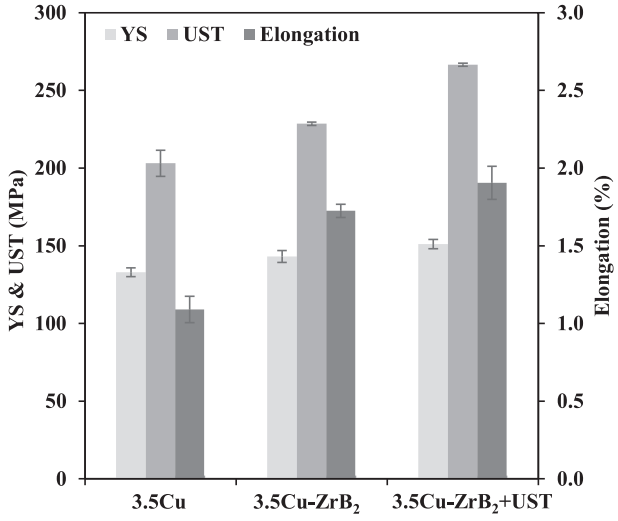

Fig. 13 – Tensile properties at room temperature of base alloy and AA4032-3.5Cu–ZrB_2 composites.

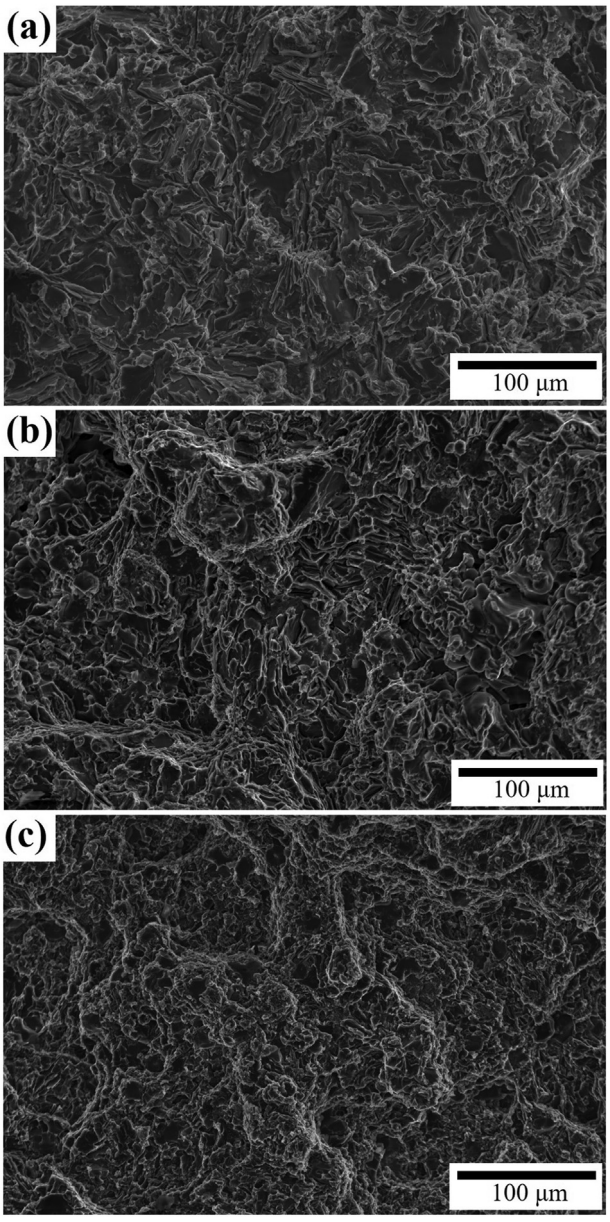

Fig. 14 – SEM micrographs of tensile fracture surfaces of (a) AA4032-3.5Cu, (b) AA4032-3.5Cu–ZrB_2 without UST, and (c) AA4032-3.5Cu–ZrB_2 with UST.

heterogeneity further. The UST lessened ZrB_2 aggregation and the ZrB_2 particles were distributed more uniformly (Figs. 11 and 15).

The strengthening mechanisms of particle reinforced aluminum matrix composites are typically listed as grain refinement strengthening ($\Delta\sigma_{GR}$), Orowan strengthening ($\Delta\sigma_{Orowan}$), dislocation strengthening ($\Delta\sigma_{Dislocation}$) and load-bearing strengthening ($\Delta\sigma_{Load}$) [39]. Among those, the Hall-Petch grain refinement and Orowan dislocation mechanisms are hardly applicable to heterogenous materials like high-Si alloys and composites based on these alloys. It has been shown that the thermal mismatch can be a contributor to the reinforcing effect, which may be attributed to the significant CTE mismatch that exists between the ZrB_2 reinforced particles (*a*-axis direction is $6.66 \times 10^{-6}\ K^{-1}$ and *c*-axis direction is $6.93 \times 10^{-6}\ K^{-1}$ [40]) and the aluminum matrix ($23 \times 10^{-6}\ K^{-1}$). This contribution is more effective in composites with UST because UST breaks the agglomerates into smaller sizes and distributes them evenly in the matrix. An increasing of the tensile strength of aluminum composite may be also related to the load bearing strengthening, which causes a load transfer to the reinforcement through interfaces between the ZrB_2 particles and AA4032 matrix [41]. In addition, the simultaneous increase of strength and ductility shows that there is another mechanism in play, i.e., delayed fracture due to the more even stress distribution upon deformation. Previous work reported that the nano-particles of ZrB_2 effectively changed the path of microcrack propagation and resulted in crack branching and deflection, slowing crack propagation and effectively increasing fracture resistance [42]. This corresponds to our result shown in Fig. 15b, revealing the ZrB_2 particles on the edge of boundary cracks that may impede the crack propagation rate and consume more fracture energy, thereby improving the fracture toughness (or strength and ductility simultaneously). In general, the increased heterogeneity of the structure that contains a soft matrix (Al) and hard phases (intermetallics and/or nonmetallic compounds) results in a more even stress distribution, preventing (paradoxically) stress concentration and delaying the catastrophic crack propagation [43,44].

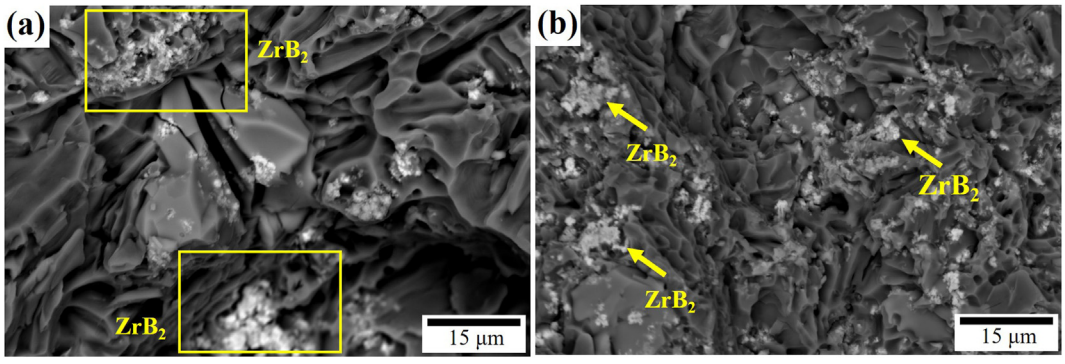

Fig. 15 – SEM micrographs of tensile fracture surfaces of AA4032-3.5Cu–ZrB_2 composite prepared (a) without UST, and (b) with UST.

5. Conclusions

The in-situ 5 wt% ZrB_2/AA4032 with high Cu composite was successfully fabricated by reaction of the molten base Al alloy with K_2ZrF_6–KBF_4 salt mixture via mechanical stirring followed by ultrasonic treatment (UST). The following conclusions can be summarized from the present study.

- Structure refinement can be achieved through the formation of ZrB_2 nanoparticles through salt synthesis. UST results the additional structure refinement.
- The formation of Si_2Zr in the AA4032-3.5Cu alloy with ZrB_2 resulted in less primary Si in the alloy.
- UST decreased the agglomeration and improved the distribution of in-situ ZrB_2 nanoparticles in AA4032-3.5Cu–ZrB_2 composites.
- UST of the composite melt improves yield strength, tensile strength, and elongation by about 5%, 15% and 10%, respectively, as compared to the composites prepared without UST.
- The structure refinement can be explained through a synergetic combination the following mechanisms: hindering grain growth by the borides, deagglomeration and refinement of additional phases by cavitation, refinement of eutectics by the overall structure refinement with a potential contribution of residual potassium.
- The improvement of tensile properties is likely to be caused by the combination of load-bearing, thermal expansion mismatch and delayed fracture mechanisms.

Author contributions

S. Chankitmunkong: Conceptualization, Methodology, Formal analysis, Writing - original draft, Writing - review & editing, Funding acquisition. **D.G. Eskin**: Writing - review & editing. **C. Limmaneevichitr**: Writing - review & editing. **P. Pandee**: Conceptualization, Methodology, Formal analysis, Writing - original draft, Writing - review & editing, Funding acquisition.

Declaration of competing interest

The authors declare that they have no known competing financial interests or personal relationships that could have appeared to influence the work reported in this paper.

Acknowledgements

The research was sponsored by the Research Strengthening Project of the Faculty of Engineering, King Mongkut's University of Technology Thonburi. SC acknowledges the financial support from King Mongkut's Institute of Technology Ladkrabang (2564-02-01-007). We are grateful for the support received from the FE-SEM center, School of Engineering, King Mongkut's Institute of Technology Ladkrabang.

REFERENCES

[1] Chankitmunkong S, Eskin DG, Patakham U, Limmaneevichitr C. Microstructure and elevated temperature mechanical properties of a direct-chill cast AA4032 alloy with copper and erbium additions. J Alloys Compd 2019;782:865–74. https://doi.org/10.1016/j.jallcom.2018.12.195.

[2] Zuo L, Ye B, Feng J, Kong X, Jiang H, Ding W. Effect of Q-$Al_5Cu_2Mg_8Si_6$ phase on mechanical properties of Al-Si-Cu-Mg alloy at elevated temperature. Mater Sci Eng, A 2017;693:26–32. https://doi.org/10.1016/j.msea.2017.03.087.

[3] Zuo L, Ye B, Feng J, Xu X, Kong X, Jiang H. Effect of δ-Al_3CuNi phase and thermal exposure on microstructure and mechanical properties of Al-Si-Cu-Ni alloys. J Alloys Compd 2019;791:1015–24. https://doi.org/10.1016/j.jallcom.2019.03.412.

[4] Yang Y, Yu K, Li Y, Zhao D, Liu X. Evolution of nickel-rich phases in Al–Si–Cu–Ni–Mg piston alloys with different Cu additions. Mater Des 2012;33:220–5. https://doi.org/10.1016/j.matdes.2011.06.058.

[5] Pramod S, Bakshi SR, Murty B. Aluminum-based cast in situ composites: a review. J Mater Eng Perform 2015;24(6):2185–207. https://doi.org/10.1007/s11665-015-1424-2.

[6] Guo S-Q. Densification of ZrB_2-based composites and their mechanical and physical properties: a review. J Eur Ceram Soc 2009;29(6):995–1011. https://doi.org/10.1016/j.jeurceramsoc.2008.11.008.

[7] Sivakumar S, Golla BR, Rajulapati KV. Influence of ZrB_2 hard ceramic reinforcement on mechanical and wear properties of aluminum. Ceram Int 2019;45(6):7055–70. https://doi.org/10.1016/j.ceramint.2018.12.208.

[8] Kaku SMY, Khanra AK, Davidson MJ. Effect of deformation on properties of Al/Al-alloy ZrB_2 powder metallurgy composite. J Alloys Compd 2018;747:666–75. https://doi.org/10.1016/j.jallcom.2018.03.088.

[9] Muralidharan N, Chockalingam K, Dinaharan I, Kalaiselvan K. Microstructure and mechanical behavior of AA2024 aluminum matrix composites reinforced with in situ synthesized ZrB_2 particles. J Alloys Compd 2018;735:2167–74. https://doi.org/10.1016/j.jallcom.2017.11.371.

[10] Kumar N, Gautam RK, Mohan S. In-situ development of ZrB_2 particles and their effect on microstructure and mechanical properties of AA5052 metal-matrix composites. Mater Des 2015;80:129–36. https://doi.org/10.1016/j.matdes.2015.05.020.

[11] Kumar NM, Kumaraswamidhas LA. Characterization and tribological analysis on AA 6061 reinforced with AlN and ZrB_2 in situ composites. J Mater Res Technol 2019;8(1):969–80. https://doi.org/10.1016/j.jmrt.2018.07.008.

[12] Zhang Z, Zhao Y, Wang C, Tao R, Fang Z, Sun Y, Kai X. High cycle fatigue behavior of in-situ ZrB_2/AA6111 composites. Mater Sci Eng, A 2020;788:139590. https://doi.org/10.1016/j.msea.2020.139590.

[13] Huang L, Zhao Y, Kai X, Cao R, Tao R, Qian W, Guan C. The effects of in-situ ZrB2 particles and Gd on the solidification behavior and mechanical properties of AA6111 matrix composites. J Mater Res Technol 2021;15:278–91. https://doi.org/10.1016/j.jmrt.2021.08.025.

[14] Selvam JDR, Dinaharan I. In situ formation of ZrB_2 particulates and their influence on microstructure and tensile behavior of AA7075 aluminum matrix composites. Eng Sci Technol Int J 2017;20(1):187–96. https://doi.org/10.1016/j.jestch.2016.09.006.

[15] Prasad L, Kumar N, Yadav A, Kumar A, Kumar V, Winczek J. In situ formation of ZrB_2 and its influence on wear and mechanical properties of ADC12 alloy mixed matrix

composites. Materials 2021;14(9):2141. https://doi.org/10.3390/ma14092141.
[16] Li H, Jiao L, Huang X, Li F, Lu S, Li Y, Li C, Qiao Y. Effect of in situ reaction temperature on the microstructure and mechanical properties of 3 wt.% ZrB_2/A356. J Mater Eng Perform 2021;30:7295–305. https://doi.org/10.1007/s11665-021-05943-6.
[17] Kai X, Huang S, Wu L, Tao R, Peng Y, Mao Z, Chen F, Li G, Chen G, Zhao Y. High strength and high creep resistant ZrB_2/Al nanocomposites fabricated by ultrasonic-chemical in-situ reaction. J Mater Sci Technol 2019;35(9):2107–14. https://doi.org/10.1016/j.jmst.2019.04.020.
[18] Kumar GN, Narayanasamy R, Natarajan S, Babu SK, Sivaprasad K, Sivasankaran S. Dry sliding wear behaviour of AA 6351-ZrB2 in situ composite at room temperature. Mater Des 2010;31(3):1526–32. https://doi.org/10.1016/j.matdes.2009.09.017.
[19] Eskin D, Tzanakis I, Wang F, Lebon G, Subroto T, Pericleous K, Mi J. Fundamental studies of ultrasonic melt processing. Ultrason Sonochem 2019;52:455–67. https://doi.org/10.1016/j.ultsonch.2018.12.028.
[20] Mohanty P, Mahapatra R, Padhi P, Ramana CV, Mishra DK. Ultrasonic cavitation: an approach to synthesize uniformly dispersed metal matrix nanocomposites—a review. Nano-Struct Nano-Objects 2020;23:100475. https://doi.org/10.1016/j.nanoso.2020.100475.
[21] Eskin GI, Eskin DG. Ultrasonic treatment of light alloy melts. CRC Press; 2017.
[22] Gupta R, Daniel B. Strengthening mechanisms in Al_3Zr-reinforced aluminum composite prepared by ultrasonic assisted casting. J Mater Eng Perform 2021;30(4):2504–13. https://doi.org/10.1007/s11665-021-05558-x.
[23] Liu J, Liu Z, Dong Z, Cheng X, Zheng Q, Li J, Zuo S, Huang Z, Gao Y, Xing J. On the preparation and mechanical properties of in situ small-sized TiB_2/Al-4.5 Cu composites via ultrasound assisted RD method. J Alloys Compd 2018;765:1008–17. https://doi.org/10.1016/j.jallcom.2018.06.303.
[24] Sheelwant A, Dutta S, Sonti KS, Narala SKR. Processing and performance assessment of particulate TiB_2 reinforced aluminum MMC developed via a novel hybrid ultrasonic casting system. Mater Manuf Process 2022;37(2):186–96. https://doi.org/10.1080/10426914.2021.1960996.
[25] Kumar HP, Xavior MA, Ashwath P. Ultrasonication and microwave processing of aluminum alloy-Graphene-Al_2O_3 nanocomposite. Mater Manuf Process 2018;33(1):13–8. https://doi.org/10.1080/10426914.2016.1244852.
[26] Tao R, Zhao Y, Kai X, Zhao Z, Ding R, Liang L, Xu W. Microstructures and properties of in situ ZrB_2/AA6111 composites synthesized under a coupled magnetic and ultrasonic field. J Alloys Compd 2018;754:114–23. https://doi.org/10.1016/j.jallcom.2018.04.282.
[27] Sreekumar V, Babu NH, Eskin D, Fan Z. Structure–property analysis of in-situ Al–$MgAl_2O_4$ metal matrix composites synthesized using ultrasonic cavitation. Mater Sci Eng, A 2015;628:30–40. https://doi.org/10.1016/j.msea.2015.01.029.
[28] Liu Z, Han Q, Li J. Fabrication of in situ Al_3Ti/Al composites by using ultrasound assisted direct reaction between solid Ti powders and liquid Al. Powder Technol 2013;247:55–9. https://doi.org/10.1016/j.powtec.2013.07.005.
[29] Kai X, Tian K, Wang C, Jiao L, Chen G, Zhao Y. Effects of ultrasonic vibration on the microstructure and tensile properties of the nano ZrB_2/2024Al composites synthesized by direct melt reaction. J Alloys Compd 2016;668:121–7. https://doi.org/10.1016/j.jallcom.2016.01.152.
[30] Hirano T, Ohtani H, Hasebe M. Thermodynamic analysis of the Al-Si-Zr ternary system. High Temp Mater Processes 2010;29(5–6):347–72. https://doi.org/10.1515/HTMP.2010.29.5-6.347.
[31] Priyadarshi A, Khavari M, Subroto T, Prentice P, Pericleous K, Eskin D, Durodola J, Tzanakis I. Mechanisms of ultrasonic de-agglomeration of oxides through in-situ high-speed observations and acoustic measurements. Ultrason Sonochem 2021;79:105792. https://doi.org/10.1016/j.ultsonch.2021.105792.
[32] Ferguson JB, Lopez HF, Rohatgi PK, Cho K, Kim C-S. Impact of volume fraction and size of reinforcement particles on the grain size in metal–matrix micro and nanocomposites. Metall Mater Trans A 2014;45(9):4055–61. https://doi.org/10.1007/s11661-014-2358-2.
[33] Tao R, Zhao Y, Kai X, Zhao Z, Ding R, Liang L, Xu W. Effects of hot rolling deformation on the microstructure and tensile properties of an in situ-generated ZrB_2 nanoparticle-reinforced AA6111 composite. Mater Sci Eng, A 2018;732:138–47. https://doi.org/10.1016/j.msea.2018.06.107.
[34] Pandee P, Sankanit P, Uthaisangsuk V. Structure-mechanical property relationships of in-situ A356/Al_3Zr composites. Mater Sci Eng, A 2023:144673. https://doi.org/10.1016/j.msea.2023.144673.
[35] Hegde S, Prabhu K. Modification of eutectic silicon in Al–Si alloys. J Mater Sci 2008;43(9):3009–27. https://doi.org/10.1007/s10853-008-2505-5.
[36] Makhlouf MM, Guthy HV. The aluminum–silicon eutectic reaction: mechanisms and crystallography. J Light Met 2001;1(4):199–218. https://doi.org/10.1016/S1471-5317(02)00003-2.
[37] Gupta N, Basu B. Hot pressing and spark plasma sintering techniques of intermetallic matrix composites. Intermetal Matrix Compos 2018:243–302. https://doi.org/10.1016/B978-0-85709-346-2.00010-8.
[38] Jayakody Mudiyanselage YC, Ramachandran K, Daniel Jayaseelan D. Fabrication and characterisation of $ZrSi_2$ ceramics via reactive hot-pressing. Adv Appl Ceram 2022:1–11. https://doi.org/10.1080/17436753.2022.2139448.
[39] Chen G, Wan J, He N, Zhang H-m, Han F, Zhang Y-m. Strengthening mechanisms based on reinforcement distribution uniformity for particle reinforced aluminum matrix composites. Trans Nonferrous Metals Soc China 2018;28(12):2395–400. https://doi.org/10.1016/S1003-6326(18)64885-X.
[40] Okamoto NL, Kusakari M, Tanaka K, Inui H, Yamaguchi M, Otani S. Temperature dependence of thermal expansion and elastic constants of single crystals of ZrB_2 and the suitability of ZrB_2 as a substrate for GaN film. J Appl Phys 2003;93(1):88–93. https://doi.org/10.1063/1.1525404.
[41] Zhang Z, Chen G, Zhang S, Zhao Y, Yang R, Liu M. Enhanced strength and ductility in ZrB_2/2024Al nanocomposite with a quasi-network architecture. J Alloys Compd 2019;778:833–8. https://doi.org/10.1016/j.jallcom.2018.11.214.
[42] Pineau A. Crossing grain boundaries in metals by slip bands, cleavage and fatigue cracks. Philos Trans Math Phys Eng Sci 2015;373(2038):20140131. https://doi.org/10.1098/rsta.2014.0131.
[43] Ma E, Zhu T. Towards strength–ductility synergy through the design of heterogeneous nanostructures in metals. Mater Today 2017;20(6):323–31. https://doi.org/10.1016/j.mattod.2017.02.003.
[44] Ashby M. The deformation of plastically non-homogeneous materials. Philos Mag: J Theor Exp Appl Phys 1970;21(170):399–424. https://doi.org/10.1080/14786437008238426.